# Two-Stage Scheduling Optimization of Grid-connected Hybrid Energy Microgrid Considering the Integration of Electric Vehicles

Weixing Ma, Yiwei Ma, Fuchun Deng

***Abstract*—In order to actively address the dual crisis of energy and climate, the current power grid system needs innovative methods to integrate renewable energy and meet the growing demand for electric vehicles (EVs). Therefore, a two-stage scheduling optimization scheme for a grid-connected hybrid energy microgrid considering the integration of EVs is proposed in this paper. In the first stage, an EVs-ordered charging and discharging strategy considering the subjective charging willingness of electric vehicle users is proposed, as well as a dual objective EV charging and discharging optimization scheduling model that considers the lowest charging cost and the closest charging amount to the expected State of Charge (SOC). In the second stage, a multi-source collaborative scheduling model and corresponding scheduling strategy among photovoltaics (PV), wind turbine (WT), energy storage system (ESS), and power grid are proposed to achieve maximum economic benefits. The results show that the proposed method can fully meet the charging demands of EVs and greatly improve system economic benefits. Compared with other scheduling models, the economic benefits have increased by 6.55%-18.54%.**

***Index Terms*—electric vehicles (EVs), grid-connected hybrid energy microgrid, economic benefits, multi-source collaborative scheduling**

## I. Introduction

With the widespread use of new energy, countries around the world are increasing the proportion of renewable distribution generations (DGs) such as solar and wind power connected to the grid [1], [2]. DGs supply to the microgrid nearby can reduce long-distance transportation of the power grid and reduce transmission line losses. photovoltaics (PV) and wind turbine (WT) generations are greatly affected by the environment and seasonality, and making power generation intermittent and uncontrollable. [3], [4]. Relying solely on DGs cannot ensure the power supply and demand balance principle of the microgrid system, which can easily lead to the waste of DGs. With the large-scale entry of electric vehicles (EVs) into the market, on the one hand, the disorderly charging of large-scale EVs will cause a load impact on the distribution network, which may have adverse effects on the operation of the power grid [5], [6]. On the other hand, the development of Vehicle to Grid (V2G) technology enables EVs to better participate in power grid scheduling [7].

The deployment of renewable DGs, energy storage systems (ESS) combined with EVs can reduce the load consumed by Microgrid from the power grid and improve the operational economy of microgrid [8]. On the other hand, the integration of hybrid energy complicates the configuration and management of microgrid. Because microgrid need to coordinate the charging/discharging power scheduling of EVs, as well as the power distribution between renewable DGs, ESS, and power grid [9]. These issues pose challenges to microgrid energy management systems (MEMS).

In recent years, numerous research achievements have been made in the orderly charging/discharging scheduling of EVs and power allocation of DGs. Chen et al. [10] proposed a real-time optimization scheduling method for EVs based on the dynamic non-cooperative game approach, which introduces the dynamic non-cooperative game method into the real-time operating system of EVs and proves the existence of a Nash equilibrium unique solution. Tan et al. [11] proposed an EV charging scheduling optimization that considers waiting time and operating costs, effectively reducing the total waiting time and individual maximum waiting time. Some optimization scheduling schemes for EVs are based on machine learning [12], [13], [14]. Wan et al. [12] proposed a model-free real-time charging scheduling for EVs based on deep reinforcement learning, and did not consider the discharge of EVs. Shang et al. [13] proposed an efficient adaptive V2G scheduling based on LSTM, and proposed a distributed edge computing framework to ensure efficient V2G scheduling. Wang et al. [14] proposed an EV prediction and scheduling framework that considers user behavior uncertainty, combining PV with a given capacity to reduce energy costs. The implementation of the appeal plan heavily relies on predicting uncertain factors such as the charging load demand of EVs (CLDE) and renewable DGs [15], [16]. The scheduling strategies for integrated energy systems (IES) are proposed in Ref. [17] and [18]. Zhang et al. [17] considered source load coordination and a tiered carbon trading mechanism, providing a feasible solution for

Manuscript received Aug 18, 2024; revised Dec 30, 2024.

This work was supported in part by the National Natural Science Foundation of China under Grant 61703068, in part by the Science and Technology Research Program of Chongqing Municipal Education Commission under Grant KJQN202304206, and in part by the Chongqing Postgraduate Research and Innovation Project under Grant CYS23468& CYS23469.

Ma Weixing is a graduate student at the School of Automation, Chongqing University of Posts and Telecommunications, Chongqing 400065, China. (e-mail: S220303008@stu.cqupt.edu.cn).

Yiwei Ma is an associate professor at the School of Automation, Chongqing University of Posts and Telecommunications, Chongqing 400065, China. (corresponding author to provide phone: +8615923177801; e-mail: mayw@cqupt.edu.cn).

Fuchun Deng is a lecturer at Chongqing University of Finance and Economics, Chongqing 402160, China. (e-mail: 1225735111@qq.com).

optimizing the scheduling of IES. Li et al. [18] established a new dual-layer optimal scheduling model for community IES under multi- stakeholder scenarios.

Furthermore, in-depth research has been conducted on the coordinated scheduling of EVs and renewable DGs. Wang et al. [19] proposed a two-stage charging mechanism for EVs, which determines the EV charging strategy by predicting the renewable DGs and CLDE. Huang et al. [20] proposed a robust scheduling method for EVs, which considers the prediction error of WT generation and improves scheduling performance under worst-case scenarios. Fakhari et al. [21] proposed a collaborative control method for renewable energy and EVs based on microgrids. Refs. [22]-[23] propose scheduling strategies for EVs in PV charging stations, Sun et al. [22] proposed an EV-PV coordination strategy based on reinforcement learning, which provides a real-time controlled EV-PV coordination strategy by predicting PV output and EV arrival in the short term. Yan et al. [23] used game theory to determine the power allocation of PV, ESS, and the power grid, as well as the total charging power of EVs, to coordinate the charging power allocation among various EVs.

There are two issues with the current research: 1) The CLDE relies on uncertain predictions, which may lead to suboptimal results and even be unable to be directly applied to practical situations. 2) The power allocation of the system only considers the current CLDE, ignoring the CLDE in subsequent periods, resulting in low economic benefits of renewable DGs power allocation and even leading to power abandonment. This article proposes a two-stage multi-dimensional collaborative scheduling scheme for the appeal issue. In stage I, establish an orderly charging /discharging scheduling model of EVs that minimizes user charging costs and meets user travel needs, and calculate the CLDE that can be determined within the microgrid system at this time. In stage II, based on the CLDE determined in the first stage, the goal is to maximize the economic benefits of renewable DGs and coordinate the power allocation of DGs. Optimize and solve the two stages using the COA algorithm.

The main contributions of this article are as follows:

1) A two-stage scheduling optimization scheme of grid-connected Hybrid Energy Microgrid has been proposed, which utilizes COA to optimize and solve the economic allocation problem of renewable DGs and the high cost of disorderly charging for EV users.

2) Based on the TOU mechanism, the EVs charging /discharging operate coefficient (CDOC) is introduced, combined with battery loss, to establish a dual objective function that minimizes charging costs and maximizes the expected amount of charging power, achieving orderly charging/discharging power, as well as advance calculation of charging costs and charging power for EVs.

3) Based on the actual situation of PV, WT, and ESS combined with the pre-calculated CLDE, the discharge operate coefficient of the ESS (DOCE) is introduced to establish the objective function with the highest DGs revenue, and to achieve power allocation optimization of DGs within the known range of the microgrid.

The rest of this article is organized as follows: Provide the basic model of the microgrid system in Section II. Section III presents the first stage EVs scheduling scheme and the second stage DGs power allocation optimization scheme. In section IV demonstrated the effectiveness of the proposed method through case studies. Finally, Section V concludes this article.

## II. System Basic Model

The framework for the two-stage scheduling optimization scheme of Grid-connected hybrid energy microgrid is shown in Fig.1. For the convenience of calculation, this article divides one day into $T$ periods and divides 1 hour into $\upsilon$ time periods, where $\upsilon=T/24$.

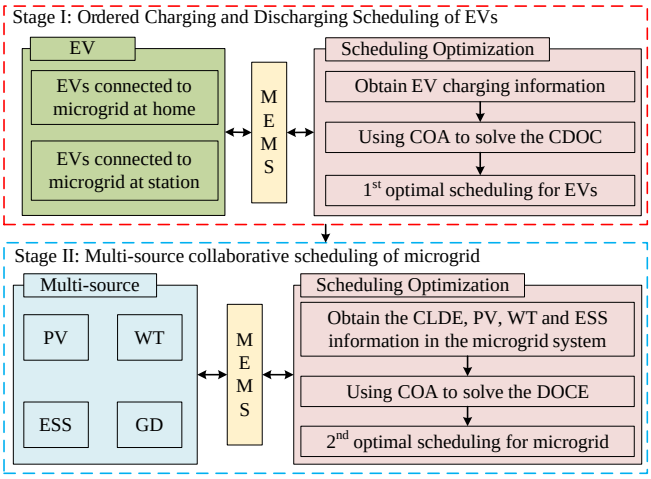


Fig. 1. The framework of the two-stage scheduling optimization scheme.

### A. Charging Behavior Model of EV

For the feasibility of EV scheduling, it is necessary to obtain information on the charging mode, charging time, and charging energy of EV [24]. The EV behavior charging models are as follows:

*(1) Classification of EV charging modes*

According to the daily use, charging power, and charging location of EVs, EV charging modes can be divided into charging EVs at home and charging EVs at charging stations. EVs have a long charging duration and low charging power at home. EVs have a short charging duration and high charging power at the station. The parameter comparison of the two charging modes of EVs is shown in Table I.

TABLE I
PARAMETERS OF DIFFERENT CHARGING MODES OF EV

| location | mode | Rated power | duration |
|---|---|---|---|
| Home | AC charging | 10kW | 4h-8h |
| Charging station | DC charging | 60kW | 0.5h-2h |

*(2) Parking duration*

There are two situations regarding the relationship between EV connection to the power grid and departure time: one is that both the connection time and departure time are completed within one day, and the other is that the grid-connection time is the previous day and the departure time is the next day. Thus, the parking time of EVs can be expressed as:

$$t_{park,k}=\begin{cases} t_{out,k}-t_{in,k}, 1<t_{in,k}<t_{out,k}<T \\ T-t_{in,k}+t_{out,k}, 1<t_{out,k}<t_{in,k}<T \end{cases} \quad (1)$$

Where, $k$ is the number of EV, $t_{park,k}$ is the parking duration of the EV$_k$, $t_{in,k}$ and $t_{out,k}$ are the time when EV$_k$ is connected/

departed to the microgrid.

*(3) Rated charging duration*

The rated charging duration of $EV_k$ is as follows:

$$t_{e,k} = \frac{(S_{e,Ek} - S_{0,Ek})C_{Ek}}{\eta_{Ec} P_{e,Ek}} \times \upsilon \tag{2}$$

Where, $t_{e,k}$ is the rated charging duration for the vehicle $EV_k$, $S_{e,Ek}$ is the expected SOC value of the EV user, $S_{0,Ek}$ is the initial SOC of the $EV_k$. $C_{Ek}$ is the battery capacity of the $EV_k$, $\eta_{Ec}$ is the charging efficiency, $P_{e,Ek}$ is the rated charging and discharging power of the $EV_k$.

*(4) Charge/discharge operate coefficient*

After being connected to the power grid, EVs will have three states: charging, discharging, and silent. To facilitate the control of the charging and discharging behavior of each EV, a CDOC is introduced:

$$X_{k,t} = zeros[x_{k,t,1}, x_{k,t,2}, ..., x_{k,t,T}] \tag{3}$$

Where, $X_{k,t}$ is the set of CDOC for $EV_k$ connected to the power grid at time *t*. *zeros* represents $X_{k,t}$ initialized as a zero vector. The elements $x_{k,t,1} \sim x_{k,t,T}$ are the CDOC of $EV_k$ connected to power grid at time *t*, used to control the charge/discharge power of $EV_k$ in each period. The control rule and the charging /discharging power of $EV_k$ is as follows:

$$\begin{cases} 0 < x_{k,t,t^v} < 1, & charge \\ x_{k,t,t^v} = 0, & silent \\ -1 < x_{k,t,t^v} < 0, & discharge \end{cases} \tag{4}$$

$$P'_{Ek} = P_{e,Ek} X_{k,t} \tag{5}$$

Where, $P'_{Ek}$ is the charging and discharging power curve of $EV_k$, $t^v = 1, 2, ..., T$ is the virtual time used for scheduling calculations.

*B. Energy Flow Model of Microgrid*

*(1) Power flow model of DGs*

Renewable DGs include PV power and WT power, DGs will supply EVs charging, ESS, and basic load of microgrid [25]. The power flow model of DGs is as follows:

$$\begin{cases} P_{DG,t} = P_{PV,t} + P_{WT,t} \\ P_{DG,t} = P_{D2L,t} + P_{D2V,t} + P_{D2E,t} \end{cases} \tag{6}$$

Where, $P_{PV,t}$ is the PV power at time *t*, $P_{WT,t}$ is the WT power generation at time *t*, $P_{D2G,t}$ is the power flow of DGs to the load (D2L) at time *t*, $P_{D2V,t}$ is the power flow of DGs to EVs charging (D2V) at time *t*, and $P_{D2E,t}$ is the power flow of DGs to the ESS at time *t*.

*(2) Power flow model of ESS*

The ESS is composed of multiple battery packs, which can meet the requirement of DGs supplying power to the ESS while the ESS supplies power to EVs. During the operation of the ESS, its energy and power flow model is as follows:

$$\begin{cases} E_{ESS,t} = E_{ESS,t-1} + \frac{P_{ESSin,t}}{\upsilon} - \frac{P_{ESSout,t}}{\upsilon} \\ P_{ESSin,t} = P_{D2E,t}, P_{ESSout,t} = P_{E2V,t} \\ S_{ESS,t} = \frac{E_{ESS,t}}{E^e_{ESS}} \end{cases} \tag{7}$$

Where, $E_{ESS,t}$ is the remaining capacity of the ESS at time *t*, $E^e_{ESS}$ is the rated capacity of the ESS, $P_{ESSin,t}$ and $P_{ESSout,t}$ respectively is the charging power and discharging power of the ESS at time *t*. $S_{ESS,t}$ is the SOC of the ESS at time *t*. $P_{E2V,t}$ is the power supplied by ESS to EVs at time *t*.

*(3) Load demand model*

The load demand is mainly composed of CLDE and the basic load demand of microgrid (BLDM). CLDE reflects the charging power of electric vehicles connected to the grid within the current and known time range The BLDM reflects the power demand of microgrid for daily life, industry, commerce, and agriculture at the current time. The load demand power balance model is as follows:

$$\begin{cases} P_{C,t} = P_{D2V,t} + P_{E2V,t} + P_{G2V,t} \\ P_{load,t} = P_{D2L,t} + P_{D,t} + P_{G2L,t} \end{cases} \tag{8}$$

Where, $P_{C,t}$ and $P_{D,t}$ are the known EVs charging power and discharging power at time *t*, respectively. $P_{V2G,t}$ is the power flowing from the EVs to the power grid at time *t*, and $P_{G2L,t}$ is the power supplied by the power grid to the load at time *t*.

*(4) Discharge control coefficient of ESS*

The ESS can charge EVs connected to the power grid. To maximize the utilization of DGs, we can store the DGs at time *t* in ESS and control the discharge behavior of ESS through MEMS to achieve power allocation of DGs at time *t*. The DOCE has been introduced to facilitate the control of DGs power allocation at time *t*, and its calculation is as follows:

$$\begin{cases} y_{t,t} = \min\{1, \frac{P_{C,t}}{P_{DG,t}}\} \\ Y_t = zeros\left[ y_{t,1}, y_{t,2}, \cdots y_{t,t^v}, ..., y_{t,T} \right] \\ y_{t,g} = 1 - \sum_{t^v=1}^{T} y_{t,t^v} \end{cases} \tag{9}$$

Where, $Y_t$ is the set of power allocation control coefficients for DGs at time *t*, $y_{t,g}$ is the allocation coefficient of DGs allocated to the power grid at time *t*, $y_{t,t}$ is the allocation coefficient of DGs allocated to EVs charging at the current time, The elements $y_{t,1} \sim y_{t,t^v}$ is the DOCE that redistributes the power flowing from DGs into ESS at time *t* to EVs within the known range of the microgrid system. The control rule is as follows:

$$\begin{cases} 0 < y_{t,t^v} \le 1, \text{discharge} \\ y_{t,t^v} = 0, \text{silent} \end{cases} \tag{10}$$

## III. Two-stage Scheduling Optimization of Microgrid

*A. Stage I- EV charging and discharging schedule*

*(1) Ordered charging and discharging scheduling strategy for electric vehicles*

When EVs are connected to the grid, the MEMS obtains the $EV_k$ 's battery capacity, and current SOC and records the time when $EV_k$ is connected to the grid [26]. At the same time, users need to input the time when the EVs depart the grid, the expected SOC at the time of departure, and whether the user responds to V2G.

Before conducting orderly charging/discharging of EVs, it

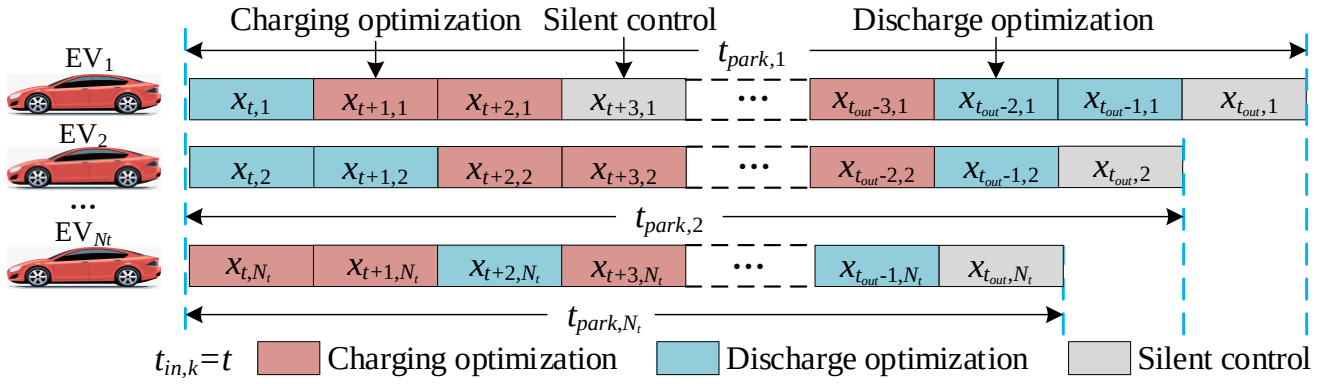


Fig. 2. Optimized charging and discharging distribution of EVs.

is necessary to first determine the relationship between the parking duration and the rated charging duration of the EVs, which are as follows:

$$\begin{cases} A_{k,t} = ones(\bullet), t_{e,k} \geq t_{park,k} \\ A_{k,t} = \mathrm{COA}(\bullet), t_{e,k} < t_{park,k} \end{cases} \tag{11}$$

$$A_{k,t} = \left\{ x_{k,t,t}, x_{k,t,t}, \cdots\cdots, x_{k,t,t_{out,k}-1} \right\} \tag{12}$$

Where, the elements in set $A_{k,t}$ correspond to the CDOC of $EV_k$ during the grid connection time, ones(•) represents making all elements of the set $A_{k,t}$ equal to 1, COA(•) represents the set $A_{k,t}$ solved by COA.

If the parking duration is shorter than the rated charging duration and the EV does not meet the conditions for orderly charging/discharging, the EV will be charged at the rated charging power. However, if the parking duration exceeds the rated charging duration and the conditions for orderly charging/discharging are met, the system will schedule the orderly charging and discharging of the EV. The distribution of optimized charging and discharging periods for EVs is shown in Fig.2.

*(2) Optimization scheduling model for EV*

*1) Objective function*

EV cycle charging/discharging can cause battery loss issues [27], and the charging/discharging costs caused by battery degradation should be taken into account. The cost of battery loss is as follows:

$$\begin{cases} C_{k,t}^{\mathrm{V2G}} = \left| \frac{B_k}{100} \right| \frac{\vartheta_{k,t}}{C_{Ek}} \rho_B \\ \vartheta_{k,t} = \max\{0, (S_{Ek,t-1} - S_{Ek,t}) C_{Ek}\} \end{cases} \tag{13}$$

Where, $C_{k,t}^{\mathrm{V2G}}$ is the battery loss cost of $EV_k$ at time $t$, $B_k$ is the linear relationship coefficient between battery life and cycle times, which is taken as 0.015 in this article; $\vartheta_{k,t}$ is the cyclic charge and discharge capacity of the $EV_k$ at time $t$, $\rho_B$ is the cost of battery replacement, $S_{Ek,t}$ is the SOC of the $EV_k$ at time $t$.

Considering the economic feasibility of user participation in orderly charging and discharging, it is advisable to allow users participating in V2G scheduling to charge during valley periods and discharge during peak periods as much as possible, achieving the scheduling effect of "peak shaving and valley filling". This approach minimize charging costs for users while meeting grid side dispatch requirements. Additionally, considering the costs associated with battery cycling, with the objective function of minimizing the charging cost of EV:

$$\begin{cases} \min f_{k,1} = \sum_{t=1}^{T} \left( \frac{x_{k,t} s_t P_{Ek}}{\upsilon} + C_{k,t}^{\mathrm{V2G}} \right) \\ s_t \in \{s_{ep}, s_p, s_f, s_v\} \end{cases} \tag{14}$$

Where, $f_{k,1}$ represents the charging and discharging cost of the $EV_k$'s after considering battery loss; $s_t$ is the charging and discharging electricity price at time t; $s_{ep}$, $s_p$, $s_f$, and $s_v$ are the charging/discharging electricity prices during extreme peak hours, peak hours, flat hours, and valley hours, respectively.

To meet the travel needs of users, the objective function is to minimize the absolute error between the actual SOC when the $EV_k$ leaves and the expected SOC:

$$\begin{cases} \min f_{k,2} = \gamma \left| S_{l,Ek} - S_{e,Ek} \right| \\ S_{l,k} = S_{0,Ek} + \frac{1}{\upsilon} \sum_{i=1}^{T} x_{k,i} \frac{P_{Ek}}{C_{Ek}} \end{cases} \tag{15}$$

Where, $f_{k,2}$ is the absolute error of SOC, $\gamma$ is a large constant, and $S_{l,Ek}$ is the SOC when EV actually leaves. Combine $f_{k,1}$ and $f_{k,2}$ to obtain the objective function of stage I:

$$\min F_{1,k} = f_{k,1} + f_{k,2} \tag{16}$$

*2) Constraint condition*

EV power constraint, EV charging and discharging cannot exceed the maximum power:

$$\begin{cases} 0 \leq P_{C,Ek,t} \leq P_{C,Ek,\max} \\ 0 \leq P_{D,Ek,t} \leq P_{D,Ek,\max} \end{cases} \tag{17}$$

Where, $P_{C,Ek,t}$ and $P_{D,Ek,t}$ respectively is the charging power and discharging power of the $EV_k$ at time $t$. $P_{C,Ek,\max}$ and $P_{D,Ek,\max}$ respectively are the maximum charging power and maximum discharging power of the $EV_k$.

Battery available capacity constraint, to avoid excessive charging and discharging of the battery, the available capacity of the battery is constrained:

$$\begin{cases} S_{Ekmin} \leq S_{Ek,t} \leq S_{Ekmax} \\ S_{Ek,t} = S_{Ek,t-1} + \frac{P_{Ek,t}^{'}}{\upsilon C_{Ek}} \end{cases} \tag{18}$$

To ensure the service life of the battery, the upper and lower limits $S_{Ekmax}$ and $S_{Ekmin}$ of the battery SOC are generally set at 1 and 0.2, respectively.

Schedulable time constraint, because the charging and discharging behavior of $EV_k$ only occurs during their grid

connection time, the CDOC of $EV_k$ before and after grid connection are both 0. $EV_k$ can only accept scheduling during the grid connection time:

$$t_{in,k} \le t_{V2G,k} \le t_{out,k} \tag{19}$$

$$\complement_{X_{k,t}} A_{k,t} = 0 \tag{20}$$

Where, $t_{V2G,k}$ is the schedulable time for $EV_k$ to participate in orderly charging/discharging, it indicates that the CDOC of EVs before and after grid connection are both 0, and the complementary elements of $A_k$ in $X_k$ are also 0.

*B. Stage II- Multi-source collaborative scheduling*

*(1) Collaborative scheduling strategy*

The basic operational goal of multi-DGs is to prioritize the use of PV power, WT power, and ESS to meet the current CLDE. If the aforementioned energy is insufficient, electricity can be purchased from the power grid to supplement. If there is surplus WT and PV power, it can be stored in ESS and supplied to the load of subsequent periods [28], thereby maximizing the utilization of PV, WT, and ESS power, reducing the operating costs of the microgrid, and minimizing dependence on the power grid.

Before executing stage II, calculate the ordered charging and discharging power of EVs after the stage I optimization. Split the optimized CDOC of $EV_k$ into optimized charging operate coefficients (COC) and discharging operate coefficients (DOC). Calculate the charging power curve and discharging power curve of the optimized $EV_k$ separately as follows:

$$\begin{cases} X'_{k,t} = X'_{C,k,t} \oplus X'_{D,k,t} \\ P'_{C,Ek,t} = P_{e,Ek} X'_{C,k,t} \\ P'_{D,Ek,t} = P_{e,Ek} X'_{D,k,t} \end{cases} \tag{21}$$

Where, $X'_{k,t}$ is the set of optimized CDOC for $EV_k$. $X'_{C,k,t}$ is the set of optimized COC for $EV_k$, and $X'_{D,k,t}$ is the set of optimized DOC for $EV_k$. $P'_{C,Ek,t}$ is the optimized charging power curve of $EV_k$, and $P'_{D,Ek,t}$ is the optimized discharging power curve of $EV_k$.

Calculate the optimized cumulative charging load curve and cumulative discharging power curve of all EVs at time $t$, that is as follows:

$$\begin{cases} P^*_{C,t} = \sum_{k=1}^{N_t} P'_{C,Ek,t} \\ P^*_{D,t} = \sum_{k=1}^{N_t} P'_{D,Ek,t} \end{cases} \tag{22}$$

$$P^*_{C,t} = [P^*_{C,t,1}, P^*_{C,t,2}, ..., P^*_{C,t,T}] \tag{23}$$

$$P^*_{D,t} = [P^*_{D,t,1}, P^*_{D,t,2}, ..., P^*_{D,t,T}] \tag{24}$$

Where, $P^*_{C,t}$ is the cumulative charging load curve of EVs connected to the grid at time $t$, $P^*_{C,t,t^v}$ is the cumulative charging load at time $t^v$ of EVs connected to the grid at time $t$. $P^*_{D,t}$ is the cumulative discharge power curve of EVs connected to the grid at time $t$, $P^*_{D,t,t^v}$ is the cumulative discharge power at time $t^v$ of EVs connected to the grid at time $t$.

Calculate the CLDE of all EV in the microgrid system at time $t$ and the known CLDE for subsequent periods in the microgrid system at time $t$ as follows:

$$\begin{cases} P^{system}_{C,t} = P^{system}_{C,t-1} + P^*_{C,t} \\ P^{system}_{C,t} = [P^{system}_{C,t,1}, P^{system}_{C,t,2}, ..., P^{system}_{C,t,T}] \end{cases} \tag{25}$$

Where, $P^{system}_{C,t}$ is the charging power curve of all EVs in the microgrid system known at time $t$, $P^{system}_{C,t,t^v}$ is the charging load at time $t^v$ of all EVs in the microgrid system known at time $t$.

Provide the following power allocation strategies for the charging demand of system EVs, the execution and scenario judgment of DGs power allocation strategy are shown in Fig.3. $S$ represents scenario code.

Scenario 1: The total power of DGs cannot meet the current CLDE. All DGs are supplied to EVs charging, and the shortfall is supplemented by the power grid.

$$\begin{cases} P_{DG,t} < P^{system}_{C,t,t} \\ S_{ESS,\min} \le S_{ESS,t} \le S_{ESS,\max} \\ P_{D2L,t} = 0, P_{G2V,t} = P^{system}_{C,t,t} - P_{DG,t} \\ P_{D2E,t} = 0, P_{D2V,t} = P_{DG,t} \end{cases} \tag{26}$$

Scenario 2: The total power of DGs just meets the current CLDE, all DGs will supply the current CLDE.

$$\begin{cases} P_{DG,t} = P^{system}_{C,t,t} \\ S_{ESS,\min} \le S_{ESS,t} \le S_{ESS,\max} \\ P_{D2L,t} = 0, P_{G2V,t} = 0 \\ P_{D2E,t} = 0, P_{D2V,t} = P_{DG,t} \end{cases} \tag{27}$$

Scenario 3: The total power of DGs can meet the CLDE at the current time and there is a surplus. The SOC of the ESS has reached the maximum allowable value and cannot be charged. At this time, the surplus DGs will be supplied to the power grid.

$$\begin{cases} P^{system}_{C,t,t} < P_{DG,t} \\ S_{ESS,t} = S_{ESS,\max} \\ P_{D2L,t} = P_{DG,t} - P_{D2V,t}, P_{G2V,t} = 0 \\ P_{D2E,t} = 0, P_{D2V,t} = P^{system}_{C,t,t} \end{cases} \tag{28}$$

Scenario 4: The total power of DGs can meet the current CLDE and exceed the total charging power of all EVs in the system. Firstly, supply DGs to meet the CLDE at the current time, then supply it to ESS to meet the CLDE in the known subsequent periods within the microgrid system and finally supply the surplus power to the power grid.

$$\begin{cases} \sum_{t^v=t}^{t+\Theta} P^{system}_{C,t,t^v} \le P_{DG,t} \\ S_{ESS,\min} < S_{ESS,t} < S_{ESS,\max} \\ P_{D2L,t} = P_{DG,t} - P_{D2E,t} - P_{D2V,t}, P_{G2V,t} = 0 \\ P_{D2E,t} = \sum_{t^v=t+1}^{t+\Theta} P^{system}_{C,t,t^v}, \ P_{D2V,t} = P^{system}_{C,t,t} \\ P_{E2V,t,t^v} = P_{DG,t} y_{t,t^v}, t^v = \{t+1, t+2, ..., t+\Theta\} \end{cases} \tag{29}$$

$$\Theta = \begin{cases} \max\{t_{out,k} - t, 1 < t_{in,k} \le t < t_{out,k} < T\} \\ \max\{t_{out,k} + 96 - t, 1 < t_{out,k} < t_{in,k} \le t < T\} \end{cases} \tag{30}$$

Where, $\Theta$ is the maximum time range from the departure

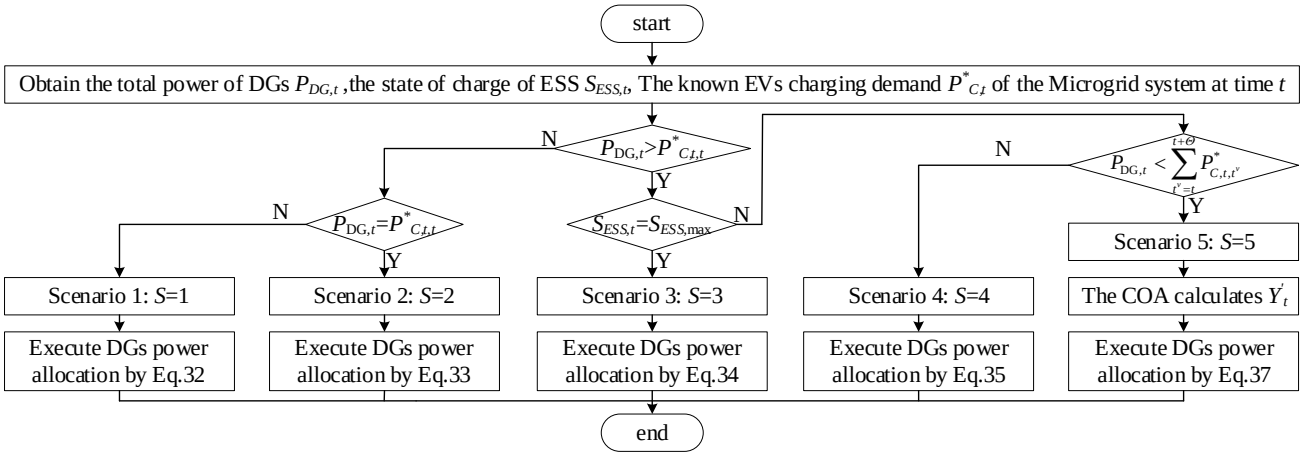


Fig .3. Collaborative scheduling execution and scene judgment process.

time of known EVs in the current system to time *t*, and as is the optimization dimension for DGs power allocation. $P_{\mathrm{E2V},t,t^v}$ is the power allocated to EVs at time $t^v$ after DGs pass through the intermediate storage of ESS at time *t*.

Scenario 5: The total power of DGs can meet the CLDE at the current time and does not exceed the total charging power of all EVs in the current system. The ESS can be charged. At this point, we will first meet the CLDE at the current time, optimize the allocation of surplus DGs to supply ESS and the power grid. Then, ESS will optimize the allocation of power obtained from DGs charging to meet the CLDE at known subsequent times in the microgrid system.

$$\begin{cases} P_{C,t,t}^{system} < P_{\mathrm{DG},t} < \sum_{t^v=t}^{t+\Theta} P_{C,t,t^v}^{system} \\ S_{ESS,\min} < S_{ESS,t} < S_{ESS,\max} \\ P_{\mathrm{D2L},t} = y_{g,t} \cdot P_{\mathrm{DG},t}, \ \ P_{\mathrm{G2V},t} = 0 \\ P_{\mathrm{D2E},t} = \sum_{t^v=t+1}^{t+\Theta} P_{\mathrm{DG},t} y_{t,t^v}, \ \ P_{\mathrm{D2V},t} = P_{C,t,t}^{system} \\ P_{\mathrm{E2V},t,t^v} = P_{\mathrm{DG},t} y_{t,t^v}, t^v = \{t+1, t+2, ..., t+\Theta\} \end{cases} \tag{31}$$

*(2) Optimization model*

*1) Objective function*

Based on the DGs allocation strategy considering CLDE in Fig.4, the DGs power allocation strategy for scenarios 1-4 can be directly executed. When in scenario 5, the power allocation of DGs needs to be optimized and solved. Considering that DGs can only sell electricity to the grid at a lower price, which is significantly lower than DGs selling electricity directly to EVs for charging, this means that charging EVs is a better way for microgrid to consume DGs than selling DGs electricity to the grid. Therefore, this article aims to maximize the economic benefits of microgrids as the objective function:

$$\min F_{2,t} = \frac{P_{\mathrm{DG},t}}{4} \left( \sum_{t^v=t}^{t+\Theta} y_{t,t^v} \cdot s_t + y_{t,g} \cdot s_{\mathrm{D2L}} \right) \tag{32}$$

Where, $F_{2,t}$ is the total revenue generated by DGs at time *t*, and $s_{\mathrm{D2L}}$ is the fixed electricity price sold by DGs to the microgrid load.

*2) Constraint condition*

Meet the power balance principle, the DGs power balance constraint is as follows:

$$P_{\mathrm{DG},t} = P_{\mathrm{D2L},t} + P_{\mathrm{D2V},t} + P_{\mathrm{D2E},t} \tag{33}$$

Operational constraints of PV/WT power systems, the PV power and WT power of the Microgrid will not exceed the upper and lower limits of the power during normal operation, which can be expressed as:

$$\begin{cases} 0 \le P_{PV,t} \le P_{PV,\max} \\ 0 \le P_{WT,t} \le P_{WT,\max} \end{cases} \tag{34}$$

Where, $P_{PV,\max}$ is the maximum power of the PV power generation system during normal operation, and $P_{WT,\max}$ is the maximum power of the WT power generation system during normal operation.

Operational constraints of ESS, the lifespan of a battery is not only related to the number of cycles and discharges but also to the depth of discharge, which constrains the available capacity of the battery. In addition, the charging and discharging power of the ESS cannot exceed the allowable range:

$$\begin{cases} 0 \le P_{ESSin,t} \le P_{ESSin,\max} \\ 0 \le P_{ESSout,t} \le P_{ESSout,\max} \\ S_{ESS,\min} < S_{ESS,t} < S_{ESS,\max} \end{cases} \tag{35}$$

To ensure the service life of the ESS, the upper and lower limits $S_{ESS,\max}$ and $S_{ESS,\min}$ of the SOC of the ESS are generally set at 1 and 0.2, respectively. $P_{ESSin,\max}$ , $P_{ESSout,\max}$ represents the maximum charging and discharging power of the ESS.

Load demand power constraint, during grid-connected operation, the purchased power of the system cannot exceed the limit of the BLDM. When DGs are allocated to EVs charging through the ESS, it cannot exceed the known EVs scheduled charging power at the microgrid system in the current:

$$\begin{cases} P_{\mathrm{E2V},t,t^v} < P_{C,t,t^v}^{system} \\ P_{\mathrm{D2L},t} + P_{\mathrm{V2G},t} \le P_{load,t} \end{cases} \tag{36}$$

*C. Two-stage scheduling optimization based on COA*

*(1) Coati Optimization Algorithm*

The Coati Optimization Algorithm (COA) was proposed by Dehghani M from the Czech Republic in 2023 [29]. In the COA optimization process, a group of randomly initialized coatis is used, simulating their behavior of hunting iguanas and escaping predators to optimize their positions. Each population consists of *N* coatis, and the current optimal individual position is considered to represent the lizard's

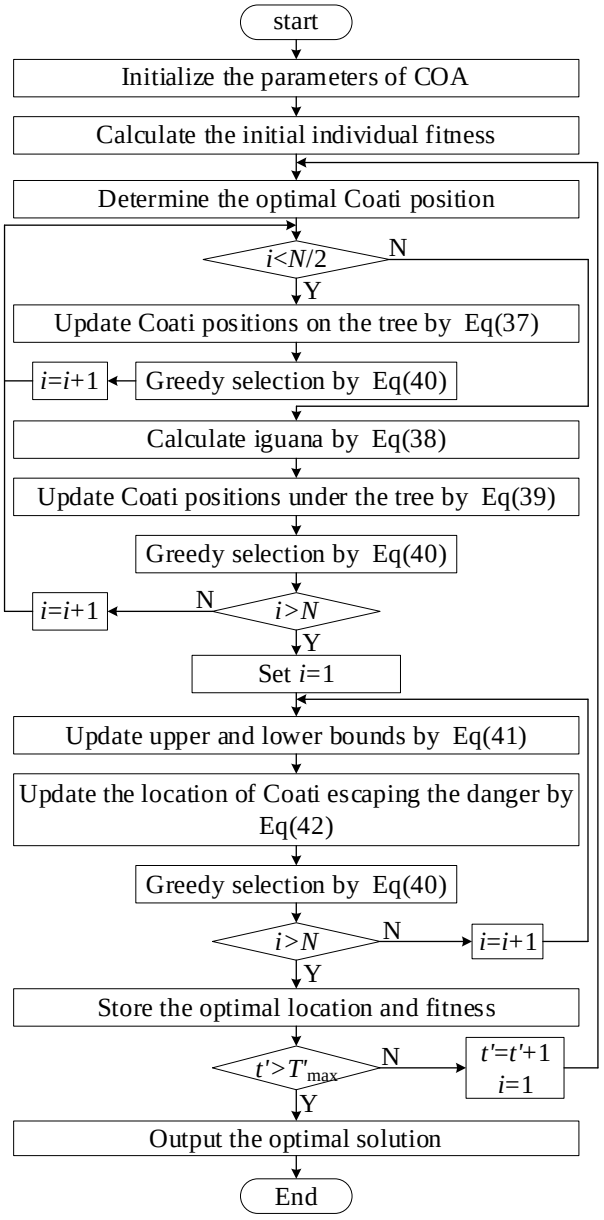


Fig. 4. The COA workflow diagram.

position. Half of the coatis climb up the tree, while the other half wait for the lizard to fall to the ground under the tree. The COA workflow diagram is shown in Fig.4.

The position update of the coatis on the tree is as follows:

$$x_i^{t'+1}(j) = x_i^{'}(j) + r \cdot (x_{best}^{t'}(j) - I \cdot x_i^{'}(j)), i = 1, 2, \cdots, \frac{N}{2} \quad (37)$$

When the lizard falls, it is placed in a random position in the search space. Based on the position of the lizard, the coati on the ground begins to move in the search space, and the position update formula is as follows:

$$iga^{t'}(j) = lb_j + r \cdot (ub_j - lb_j) \quad (38)$$

$$x_i^{t'+1}(j) = \begin{cases} x_i^{t'}(j) + r(iga^{t'}(j) - Ix_i^{t'}(j)), fit(iga^{t'}) < fit(x_i^{t'}) \\ x_i^{t'}(j) + r(x_i^{t'}(j) - iga^{t'}(j)), fit(iga^{t'}) \geq fit(x_i^{t'}) \end{cases} \quad (39)$$

$$, i = \frac{N}{2} + 1, \frac{N}{2} + 2, ..., N$$

Where, $t'$ is the current iteration count, $lb_j$ is the lower bound of the $j$-th variable, $ub_j$ is the upper bound of the $j$-th variable, and $fit(\cdot)$ is used to calculate fitness. $r$ is a random number between (0,1), and $I$ is a random integer from the set of integers {1,2}. $iga^{t'}$ is the new position of the iguana after it lands on the ground, $x_i^{t'}(j)$ is the $j$-th dimensional variable value of the $i$-th individual in the current iteration. Perform a greedy selection between the updated position and the previous position as follows:

$$x_i^{t'+1} = \begin{cases} x_i^{t'+1}, & fit(x_i^{t'+1}) < fit(x_i^{t'}) \\ x_i^{t'}, & fit(x_i^{t'+1}) \geq fit(x_i^{t'}) \end{cases} \quad (40)$$

When a predator attacks a coati, the coati will flee its location, which is the development ability of COA in local search. The location update is as follows:

$$lb_j^l = \frac{lb_j}{t'}, ub_j^l = \frac{ub_j}{t'}, t' = 1, 2, \cdots, \Gamma \quad (41)$$

$$x_i^{t'+1}(j) = x_i^{t'}(j) - (1 - 2r) \cdot (lb_j^l + r \cdot (ub_j^l - lb_j^l)), \quad i = 1, 2, ..., N \quad (42)$$

Where, $r$ is a random number between [0,1], and $\Gamma$ is the maximum number of iterations. It shows that $lb_j^l$ and $ub_j^l$ are the upper and lower bounds of the $j$-th dimensional variable that update with the number of iterations. Make a greedy choice by using (14).

Until all the iterative processes are completed, the final fitness obtained is the optimal value of the coati population.

*(2) Two-stage scheduling optimization program*

Two-stage scheduling optimization of grid-connected hybrid energy microgrid considering the integration of EVs based on COA is shown in Fig.5, The specific implementation steps are as follows:

Step 1: determine the number $N_t$ of EVs connected to the power grid at time $t$, obtain the charging information of $EV_k$ through MEMS, and initialize the CDOC of $EV_k$ to zero.

Step 2: Calculate the parking duration of the $EV_k$ and compare it with the rated parking duration by Eq.(11).

If the parking duration is less than the rated duration, charge according to the rated power.

Otherwise, the parking duration of $EV_k$ is greater than the rated duration, and the conditions for optimizing charge and discharge scheduling are met, $t_{park,k}$ is the optimization dimension for $EV_k$ to participate in orderly charge/discharge scheduling.

Step 3: Using the $X_{k,t}$ of $EV_k$ as a variable, the objective function is shown in Eq.(16), and the constraints are shown in Eq.(17) - (20). The COA is used to solve the optimized $X_{k,t}^{'}$.

Step 4: The charging and discharging power of $EV_k$ is calculated by Eq.(5). Calculate the optimized charge and discharge power curves for a single $EV_k$ by Eq.(7).

Step 5: Repeat steps 2-4 until all EVs connected to the grid at time $t$ have completed optimized scheduling.

Step 6: Calculate the cumulative charging load and cumulative discharging power of all EVs optimized at time $t$ by Eq.(22).

Step 7: Input the orderly charging/discharging scheduling results of the first stage's EVs into stage II.

Step 8: Obtain the PV and WT power generation at time $t$ through the energy meteorological station, and obtain the real-time basic load of microgrid at time $t$ from the dispatch center.

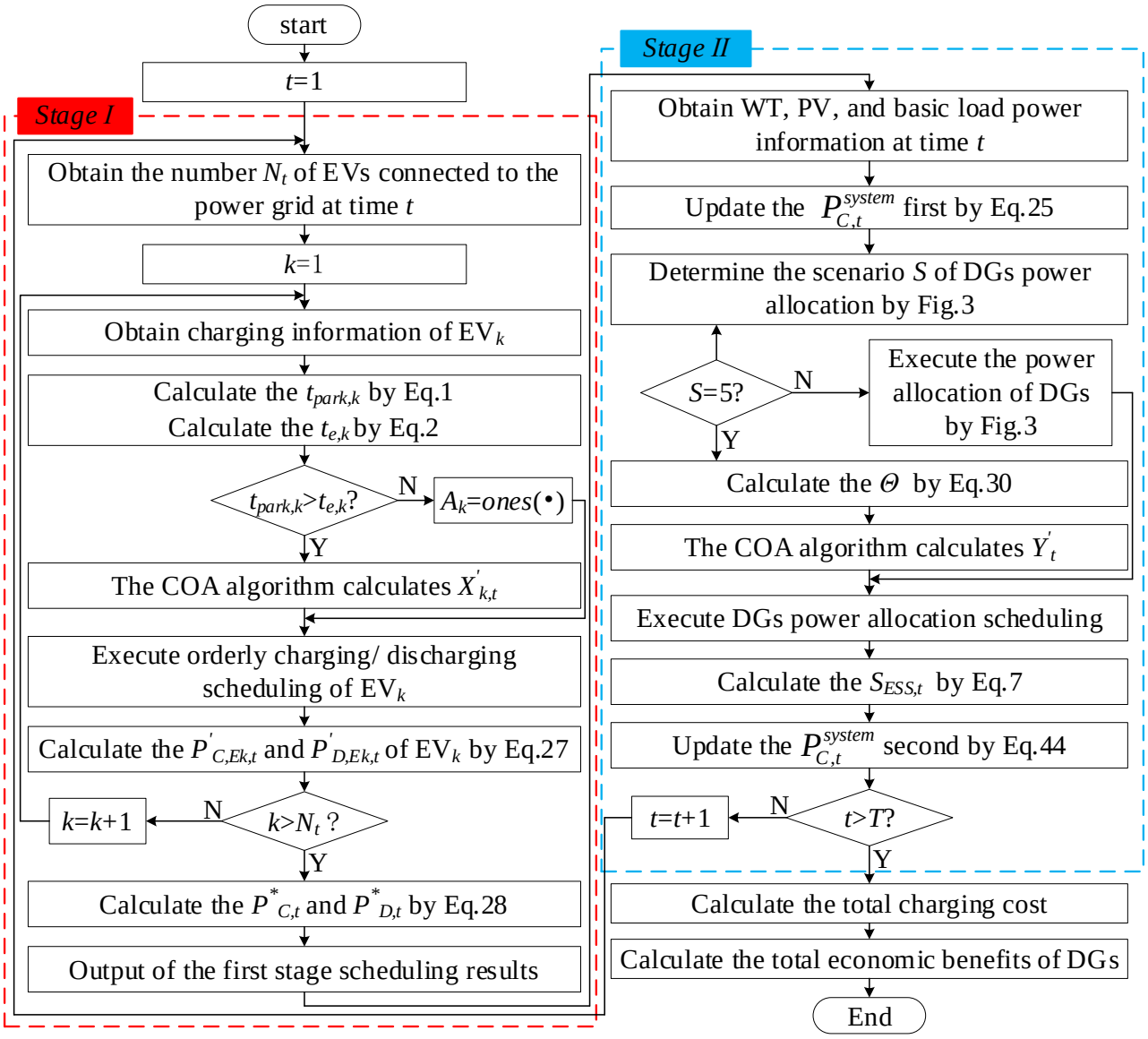


Fig. 5. Flowchart of two-stage scheduling optimization.

Step 9: Calculate the CLDE of all EVs at time $t$ and the known CLDE of subsequent periods in the microgrid system by Eq.(25).

Step 10: Based on the energy flow relationship and constraints within the system, determine the power allocation strategy for DGs by Fig.3.

If $S$ is not equal to 5, directly allocate the power of DGs by Eq.(26) - (29) and Fig.3.

Else, calculate the optimization dimension for $\Theta$ DGs power allocation by Eq.(30). Using the DOCE of ESS as a variable, the objective function is shown in Eq.(32), and the constraints are shown in Eq.(33) - (36). The COA is used to solve the optimized $Y'_t$ of ESS.

Step 11: Start executing DGs power allocation optimization scheduling by Eq.(31), and calculate the SOC of ESS at time $t$ by Eq.(7).

Step 12: Due to the optimization of DGs power allocation at time $t$, a portion of the CLDE in the system will be offset. Therefore, before allocating DGs power at time $t$+1, the CLDE in the system should subtract the offset-power at time $t$. The formula for updating CLDE in the system is as follows:

$$P^*_{\mathrm{D2V},t} = P_{\mathrm{DG},t} Y'_t \tag{43}$$

$$P^{system}_{C,t} = P^{system}_{C,t} - P^*_{\mathrm{D2V},t} \tag{44}$$

Where, $P^*_{\mathrm{D2V},t}$ is the assigned power of DGs flowing into EVs at time $t$.

Step 13: Repeat steps 1-12 until two-stage scheduling optimization is completed for all periods within a day

## I. Simulation Results and Discussion

### A. Parameter settings

An actual microgrid developed in Chongqing City is selected for experimentation verification, which includes WT, PV, ESS, load, fast charging stations, home charging poles and EVs. The corresponding parameters are as follows: (1) Microgrid: $P_{RDN,\max,t}=5000\mathrm{kW}$, $s_{\mathrm{D2G}}=0.4$ ¥, the TOU electricity price for EVs is shown in Table I, the G2L price is 70% of it. $P_{WT,\max}=1250\mathrm{kW}$, $P_{PV,\max}=880\mathrm{kW}$, $T$=96, $\upsilon$=4. (2) ESS: $E^e_{ESS}=4000\mathrm{kWh}$, $P_{ESSin,\max}=P_{ESSout,\max}=600\mathrm{kW}$. (3) EVs: There are 600 EVs in the microgrid, of which 300 EVs are connected at home and the maximum charging/ discharging power is $P_{C,Ek,\max}=P_{D,Ek,\max}=P_{e,Ek}=10\mathrm{kW}$,

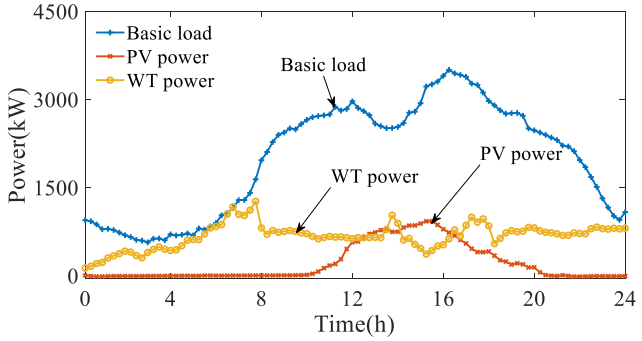


Fig. 6. Basic load and DG electricity of microgrid.

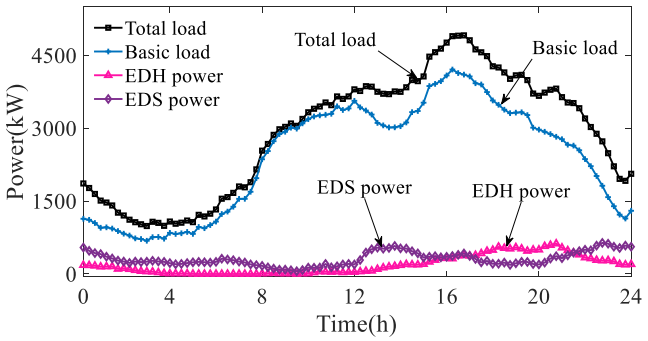


Fig. 7. Unordered charging load of EVs at different charging locations.

TABLE I
THE TOU ELECTRICITY PRICE FOR EVS

| Periods $s_t$ | Specific period | Price (¥/kWh) |
|---|---|---|
| $s_{ep}$ | 15:00-17:00 | 1.597 |
| $s_p$ | 11:00-12:00, 14:00-15:00, 17:00-21:00 | 1.332 |
| $s_f$ | 7:00-11:00, 12:00-14:00, 21:00-23:00 | 0.839 |
| $s_v$ | 23:00-7:00 | 0.489 |

and another 300 EVs are connected at stations and the maximum charging /discharging power is $P_{C,Ek,\max} = P_{D,Ek,\max} = P_{e,Ek} = 60\text{kW}$, $C_{Ek} = 60\text{kWh}$, $\eta_{Ec} = 0.95$, $B_k = 0.0156$, $\rho_B$=35000¥. (4) COA: $N$=100, Γ=200.

Fig.6 shows the basic load and distributed generation situation, and Fig.7 shows the basic load and disorderly charging EVs, which are under the following situations: EVs charging disorderly at home (EDH), EVs charging disorderly at the station (EDS). The energy integration of microgrid systems includes: Charging power of EVs at home (CEH),discharge power of EVs at home (DEH), charging power of EVs at the station (CES), discharge power of EVs at the station (DES), total power of EVs at home (TEH), the total power of EVs at the station (TES).

The disorderly charging of EVs causes the peak-to-peak effect on the basic load curve, significantly increasing the peak-to-valley difference of the basic load curve. Renewable DGs have significant power fluctuations.

### *B. Simulation result*

*1) The result of stage I scheduling optimization*

According to the stage I scheduling strategy, conduct simulation experiments on the orderly charging scheduling of EVs (OCS1) and orderly charging/discharging scheduling of EVs (OCS2), and compare them with the disordered charging of EVs (DCE). Fig.8 shows stage I optimized scheduling results of ordered EVs charging. Fig.9 shows the optimization results of orderly charge/discharge scheduling for EVs in

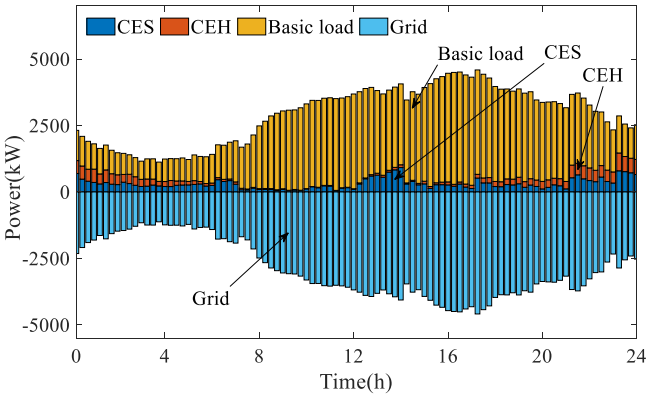


Fig. 8. The orderly charging scheduling results of EVs in stage I.

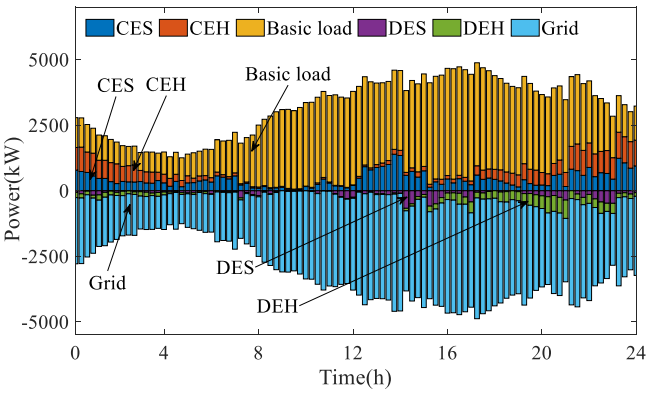


Fig.9. The orderly charging/discharging scheduling results of EVs in stage I.

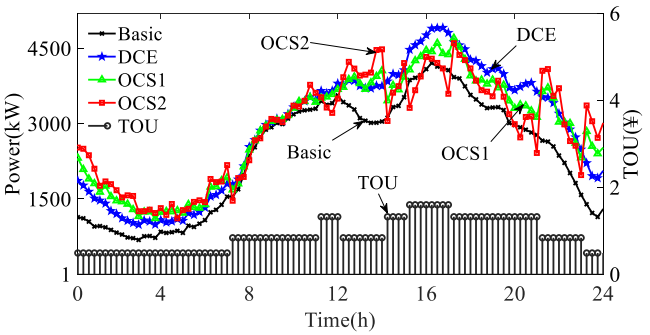


Fig. 10. Comparison results of several EVs charging methods in stage I.

stage I. Fig.10 shows the comparison results of several EVs scheduling methods. Table II presents a quantitative comparison of several EVs scheduling methods.

Fig. 8 shows that the peak charging period for EVs occurs from 12:00-14:00, 21:00 to 2:00 the next day, during periods of low electricity consumption, effectively alleviating the problem of power conflicts in microgrids.Fig.9 shows that the optimized discharge behavior of EVs is concentrated on 11:00-12:00, 15:00- 17:00, 20:00-21:00, 22:00-23:00, etc. The peak charging load of EVs is concentrated from 12:00 to 14:00, and 21:00 to 3:00 the next day. The OSM2 scheme effectively achieves V2G discharge during peak hours and charging during valley hours for EVs. Fig.9 and Fig.10, show that after executing EVs optimized charging/discharging scheduling, the peak area of the total load curve of the microgrid is significantly reduced. The power consumption in the low valley area is significantly increased. The peak-valley difference (PVD) and load variance of the microgrid have significantly decreased.

Table II shows that there is no discharge revenue or battery

TABLE II
QUANTITATIVE COMPARISON OF SEVERAL EVS SCHEDULING METHODS

| Model | Site | Cost (¥) | Income (¥) | Total cost (¥) | PVD (kW) | Variance (MW) |
|---|---|---|---|---|---|---|
| DCE | Station | 6754.12 | — | 11980.09 | 3924.74 | 1540.87 |
| | Home | 5225.97 | — | | | |
| OCS1 | Station | 6105.83 | — | 9950.80 | 3491.08 | 1139.91 |
| | Home | 3599.92 | — | | | |
| OCS2 | Station | 9458.49 | 3717.51 | **8798.54** | **3472.43** | **1044.90** |
| | Home | 7446.05 | 4388.49 | | | |

TABLE III
EVALUATION INDICATORS FOR SOC'S ABSOLUTE ERROR

| Charging Model | Location | ASE | FIP (%) | PEL (%) | MSE |
|---|---|---|---|---|---|
| OCS1 | Station | 0.0021 | 62.00 | **96.33** | **0.0383** |
| | Home | **0.0021** | **67.33** | 95.33 | 0.0556 |
| OCS2 | Station | 0.0056 | 64.67 | 86.00 | 0.0771 |
| | Home | 0.0072 | 35.63 | 77.67 | 0.0822 |

loss cost for the DCE and OCS1 scenarios. While EV users have discharge revenue for the OCS2 scenario, and EVs connected at stations have a battery loss of 274.22 (included in the cost in Table II), EVs connected at home have a battery loss of 529.88 (included in the cost in Table II). The total charging cost of OCS1 is 9950.80 ¥, corresponding to a microgrid load PVD and load variance of 3491.08 kW and 1139.91 MW, respectively. Compared with DCE, total charging cost, PVD and load variance decreased by 17.52%, 11.05%, and 26.02%, respectively. The total charging cost of OCS2 is 8798.54 ¥, corresponding to a microgrid load PVD and load variance of 3472.43kW and 1044.90MW, respectively. Compared with DCE, total charging cost, PVD and load variance have decreased by 26.56%, 11.52%, and 32.19%, respectively. Experimental results have shown that EV users' charging cost and microgrid load curves are better than DCE in both OCS1 and OCS2, and OCS2 has the best results.

Before the first inflection point (FIP), the SOC error is extremely small. We consider that the error before the FIP fully meets the SOC expectation. If the SOC error is less than 0.01, it is considered an acceptable error range for users. The average SOC error (ASE) is a reflection of the overall error size, and the maximum SOC error (MSE) is the worst-case evaluation, ASE, FIP, proportion of error less than 0.01(PEL), and MSE are used as SOC error evaluation indicators. Fig.11 shows the absolute error between SOC when the EVk leaves and the expected SOC. Fig.12 shows the cumulative probability (CP) of SOC absolute error. Table III shows the evaluation indicators for SOC absolute error distribution results.

From Fig.11-12 and Table III, it can be concluded that the range of ASE is between 0.0021-0.0072, and the converted energy is 0.126-0.42kWh. ASE is less than 0.01, energy error is less than 0.6 kWh, overall meeting the expected SOC requirements of EV users. The MSEs are 0.0383, 0.0556, 0.0771 and 0.0822, respectively, converted to energy of 2.298, 3.336, 4.626 and 4.932 kWh, respectively. Although there are a very small number of EVs whose SOC did not meet the user's expectations when leaving, the energy difference of 2.298-4.932 kWh will not affect the user's daily travel. The range of FIP is between 35.63% and 67.33%, reflecting the complete satisfaction rate of EV users with the charging

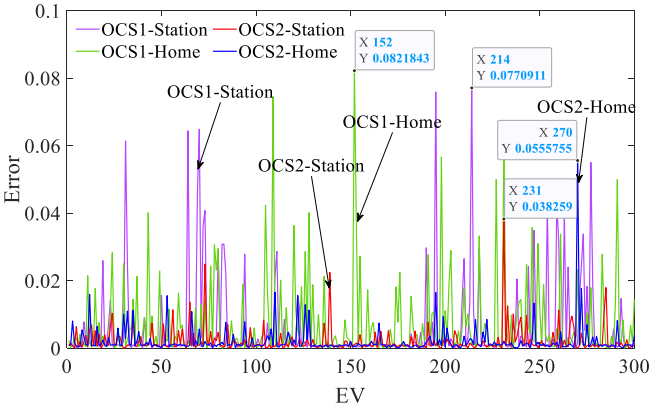


Fig. 11. The absolute error of SOC.

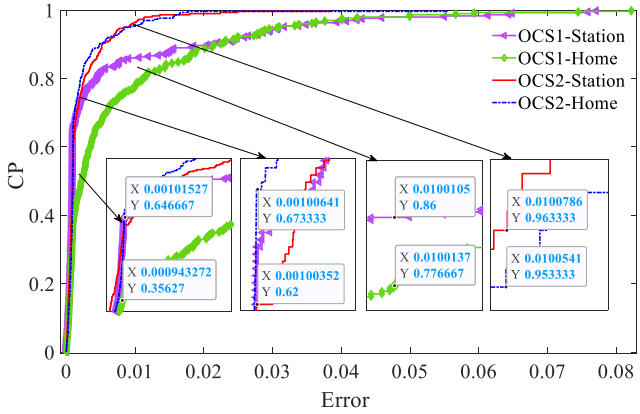


Fig. 12. Cumulative probability of SOC absolute error.

power. The range of PEL is between 77.67% and 96.33%, reflecting that the SOC of the vast majority of EV users is satisfactory after charging is completed.

*2) The result of the two-stage scheduling optimization*

To fully verify the superiority of this scheme, the two-stage scheduling optimization model (SOM6) proposed in this paper is compared with five other models: the disordered scheduling model (SOM1), stage I optimization charging scheduling model (SOM2), stage I optimization charging/ discharging scheduling optimization model (SOM3), stage II scheduling optimization model (SOM4), and the two-stage scheduling optimization model for EV charging scheduling (SOM5). Fig.13-18 show the experimental results of the SOMs, respectively. Fig.19 shows the power allocation optimization results of SOM6, and Fig.20 shows the load results of microgrids with different SOMs. Table IV shows the DGs' economic benefits of different comparison models.

Comparing Fig.13-18, SOM1, SOM2, SOM4, and SOM5 show that a large of DGs flow into the microgrid, and a large part of the charging load demand for EVs comes from the microgrid, which can lead to low economic benefits for DGs. SOM5, due to the orderly charging scheduling of EVs in the first stage, limits the charging range of EVs to valley and flat periods, and DGs mainly supply the charging load demand for EVs in valley and flat periods, resulting in low efficiency for DGs. SOM3 and SOM6, due to the discharge behavior of EVs, increase the demand for EV charging, further promoting the supply of a large number of DGs for EV charging and improving the economic benefits of DGs, the SOM3 model is not optimize the power allocation of DGs, resulting in low economic benefits for DGs. Among them, SOM6 supplies a large amount of DGs to the charging needs of EVs during

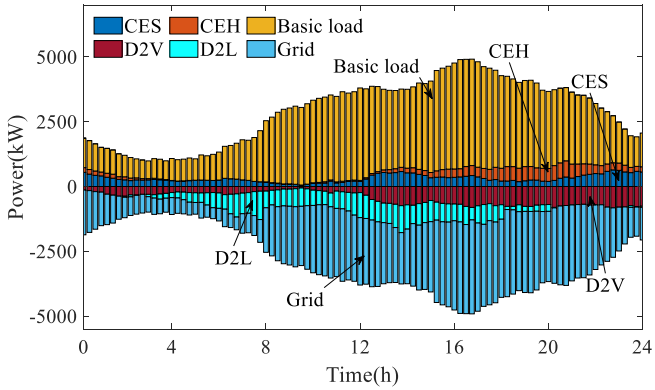


Fig. 13. Scheduling optimization results of SOM1.

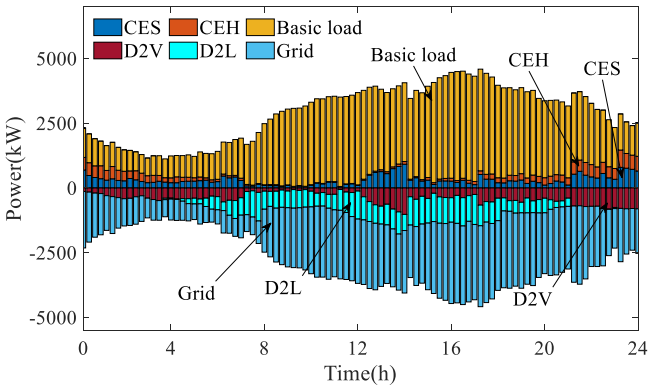


Fig. 14. Scheduling optimization results of SOM2.

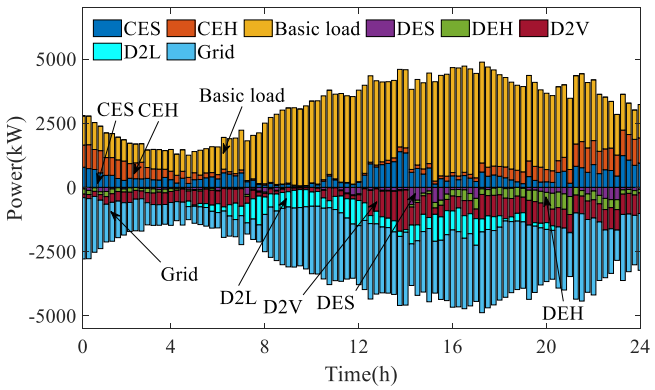


Fig. 15. Scheduling optimization results of SOM3.

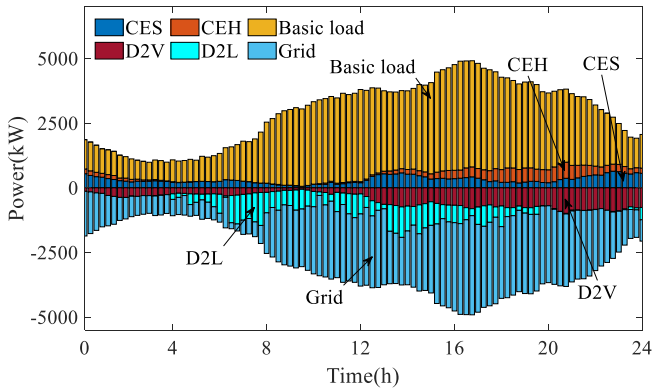


Fig. 16. Scheduling optimization results of SOM4.

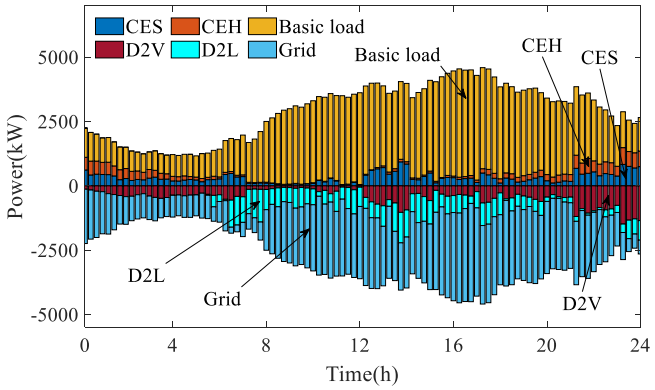


Fig. 17. Scheduling optimization results of SOM5.

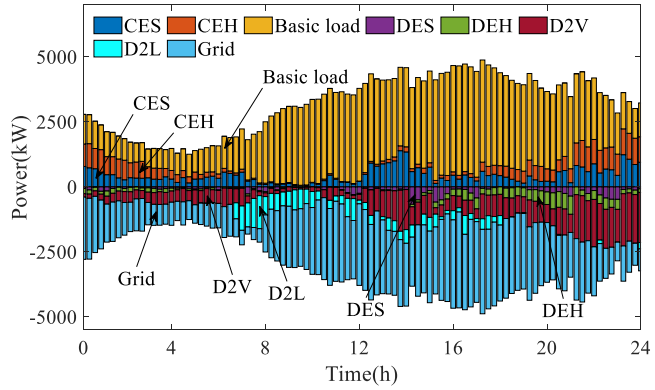


Fig .18. Scheduling optimization results of SOM6.

peak and normal periods, and the remaining power is mainly supplied to microgrid loads during the period of 7:00-11:00. The proportion of DGs consumed by EVs is much higher than that of the basic load, which can significantly improve the economic benefits of DGs.

Fig.19 shows that during the low season of DGs, the CLDE during the valley period cannot be met, and a power grid is needed for supply. However, during the peak season of DGs, not only can the current CLDE be met, but the surplus DGs can also be directed to the ESS. Especially in 13:00-20:00, the ESS stores the surplus DGs power, and in 20:00-24:00, the stored DGs power is released to meet the CLDE and supply the subsequent CLDE. The fitting evaluation index $R^2$ of the $P_{EV}$ and $P_{D2V}$ is equal to 0.9951, the charging load demand for EVs is met by the DGs, reducing the power supply of the power grid for EVs charging. Fig.20 shows that during the valley period of 0:00-6:00, the load of microgrid based on SOM6 is significantly higher than that of microgrids by other SOMs, during the peak period of 17:00-22:00, the load of microgrid based on SOM6 is significantly lower than that of microgrids by other SOMs.

Table IV shows that the D2V income of the SOM6 is higher than other SOMs, at ¥14530.44. The D2G return is significantly lower than other SOMs, at ¥2170.53. And the total income is the highest, at ¥16700.97. The microgrid load cost of SOM6 is only higher than SOM3 and lower than other SOMs. The load cost of SOM6 is relatively low at ¥32297.44, only higher than the ¥31341.35 of the SOM3. SOM6 Achieving collaborative optimization scheduling of EV and hybrid energy, improving the economic benefits of microgrid while increasing the revenue of EV users.

TABLE IV
DGS' ECONOMIC BENEFITS UNDER DIFFERENT SCHEDULING MODELS

| Scheduling Model | D2V income(¥) | D2L income(¥) | Total income(¥) | Load cost(¥) |
|---|---|---|---|---|
| SOM1 | 11307.20 | 4098.96 | 15406.16 | 33728.14 |
| SOM2 | 11060.69 | 4029.75 | 15090.44 | 32365.35 |
| SOM3 | 12408.39 | 3265.34 | 15673.73 | 31341.35 |
| SOM4 | 11712.24 | 3937.41 | 15649.65 | 33696.02 |
| SOM5 | 9430.33 | 4658.30 | 14088.63 | 33070.86 |
| SOM6 | 14530.44 | 2170.53 | **16700.97** | 32297.44 |

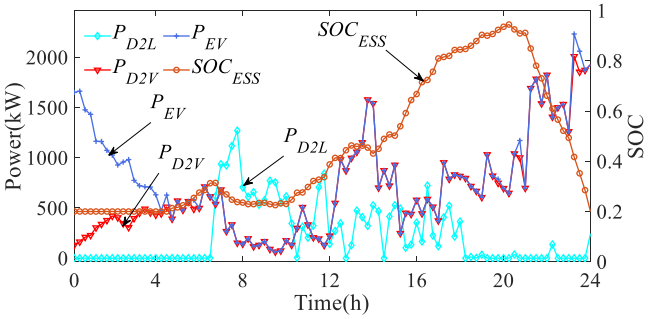


Fig. 19. power allocation optimization results of SOM6.

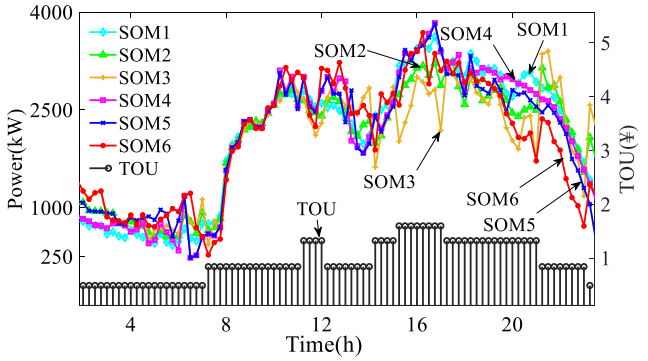


Fig. 20. Comparison results of SOMs.

## V Conclusion

This article proposes a two-stage coordinated optimization scheduling scheme for Microgrid considering DGs and EVs. Stage I considers the unique charging needs of EVs, aiming to maximize the satisfaction of EVs' charging capacity requirements without sacrificing EVs usage time, reduce EV charging costs, and solve the coordination problem of EV charging and discharging. Due to the optimization scheduling in the first stage, the CLDE has increased. In stage II, DGs power allocation allocates as much power as possible to EVs charging, solving the problem of the economic benefits of DGs. Finally, the proposed scheme was validated through simulation and experimentation. Compared with other scheduling optimization, this scheme reduces the charging cost of EVs by 17.52%-26.56%, improves user satisfaction with charging, The range of PEL is 77.76%-96.33%. And maximizes the supply of DGs to EVs' charging needs, significantly improving the economic benefits of DGs, that profit is 6.55% -18.54% higher than other scheduling models. Optimize the load curve of microgrids and reduce their operating cost operating cost is ¥32297.44. The numerical results and comparison with the benchmark validate the effectiveness of the method.

## References


[1] K. Wang, X. Qi, and H. Liu, "A comparison of day-ahead photovoltaic power forecasting models based on deep learning neural network," *Appl. Energ.*, vol. 251, no. 113315, Oct. 2019.

[2] U. K. Das, K. S. Tey, M. Seyedmahmoudian, S. Mekhilef, M. Y. I. Idris, W. V. Deventer, B. Horan, and A. Stojcevski, "Forecasting of photovoltaic power generation and model optimization: A review," *Renew. Sustain. Energy Rev.*, vol. 81, pp. 912–928, Jan. 2018.

[3] C.-J. Huang and P.-H. Kuo, "Multiple-input deep convolutional neural network model for short-term photovoltaic power forecasting," *IEEE Access*, vol. 7, pp. 74822–74834, Jun. 2019.

[4] L. Yang, M. He, J. Zhang, and V. Vittal, "Support-vector-machine-enhanced Markov model for short-term wind power forecast," *IEEE Trans. Sustain. Energ.*, vol. 6, no. 3, pp. 791–799, Jul. 2015.

[5] KAUR K, KUMAR N, SINGH M. "Coordinated power control of electric vehicles for grid frequency support: MILP-based hierarchical control design," *IEEE Trans. Smart Grid*, vol. 10, no. 3, pp. 3364–3373, May 2019.

[6] SHAFIQ S, IRSHAD U B, AL-MUHAINI M. "Reliability evaluation of composite power systems: evaluating the impact of full and plug-in hybrid electric vehicles," *IEEE Access*, vol. 8, pp. 114305–114314, Jun. 2020.

[7] PENG Chao, ZOU Jianxiao, LIAN Lian, et al. "An optimal dispatching strategy for V2G aggregator participating in supplementary frequency regulation considering EV driving demand and aggregator's benefits," *Appl. Energ.*, vol. 190, pp. 591–599, Mar. 2017.

[8] M. Mahmoodi, P. Shamsi and B. Fahimi, "Economic dispatch of a hybrid microgrid with distributed energy storage," *IEEE Trans. Smart Grid*, vol. 6, no. 6, pp. 2607–2614, Nov. 2015.

[9] W. Shi, N. Li, C. C. Chu and R. Gadh, "Real-time energy management in microgrids," *IEEE Trans. Smart Grid*, vol. 8, no. 1, pp. 228–238, Jan. 2017.

[10] L. P. Chen, T. Yu, Y. X. Chen, W. L. Guan, Y. Shi and Z. N. Pan, "Real-time optimal scheduling of large-scale electric vehicles: a dynamic non-cooperative game approach," *IEEE Access*, vol. 8, pp. 133633–133644, Jul. 2020.

[11] M. Tan, Y. Ren, R. Pan, L. Wang and J. Chen, "Fair and efficient electric vehicle charging scheduling optimization considering the maximum individual waiting time and operating cost," *IEEE Trans. Veh. Technol.*, vol. 72, no. 8, pp. 9808–9820, Aug. 2023.

[12] Z. Wan, H. Li, H. He and D. Prokhorov, "Model-free real-time EV charging scheduling based on deep reinforcement learning," *IEEE Trans. Smart Grid*, vol. 10, no. 5, pp. 5246–5257, Sept. 2019.

[13] Y. Shang, Y. Shang, H. Yu, Z. Shao and L. Jian, "Achieving efficient and adaptable dispatching for vehicle-to-grid using distributed edge computing and attention-based LSTM," *IEEE Trans. Ind. Inform.*, vol. 18, no. 10, pp. 6915-6926, Oct. 2022.

[14] B. Wang, Y. Wang, H. Nazaripouya, C. Qiu, C. C. Chu and R. Gadh, "Predictive scheduling framework for electric vehicles with uncertainties of user behaviors," *IEEE Internet Things*, vol. 4, no. 1, pp. 52–63, Feb. 2017.

[15] M. H. K. Tushar, A. W. Zeineddine and C. Assi, "Demand-side management by regulating charging and discharging of the EV, ESS, and utilizing renewable energy," *IEEE Trans. Ind. Inform.*, vol. 14, no. 1, pp. 117–126, Jan. 2018.

[16] Y. Yang, Q. S. Jia, G. Deconinck, X. H. Guan, Z. F. Qiu, and Z. C. Hu, "Distributed coordination of EV charging with renewable energy in a microgrid of buildings," *IEEE Trans. Smart Grid*, vol. 9, no. 6, pp. 6253–6264, Nov. 2018.

[17] Y. Zhang, L. Li, W. Hu. "An integrated energy demand response model considering source-load synergy and stepped carbon trading mechanism," *Engineering Letters*, vol. 32, no.3, pp. 614–624, Mar. 2024.

[18] Y. Li, M. Han, Z. Yang and G. Li, "Coordinating flexible demand response and renewable uncertainties for scheduling of community integrated energy systems with an electric vehicle charging station: a bi-level approach," *IEEE Trans. Sustain. Energ.*, vol. 12, no. 4, pp. 2321–2331, Oct. 2021.

[19] R. Wang, P. Wang and G. Xiao, "Two-stage mechanism for massive electric vehicle charging involving renewable energy," *IEEE Trans. Veh. Technol.*, vol. 65, no. 6, pp. 4159–4171, Jun. 2016.

[20] Q. Huang, Q. -S. Jia and X. Guan, "Robust scheduling of EV charging load with uncertain wind power integration," *IEEE Trans. Smart Grid*, vol. 9, no. 2, pp. 1043–1054, Mar. 2018.

[21] M. F. M. Arani and Y. A. R. I. Mohamed, "Cooperative control of wind power generator and electric vehicles for microgrid primary frequency regulation," *IEEE Trans. Smart Grid*, vol. 9, no. 6, pp. 5677–5686, Nov. 2018.

[22] F. Sun et al., "Prediction-based EV-PV coordination strategy for charging stations using reinforcement learning," *IEEE Trans. Ind. Appl.*, vol. 60, no. 1, pp. 910–919, Feb. 2024.

[23] D. Yan, H. Yin, T. Li and C. Ma, "A two-stage scheme for both power allocation and EV charging coordination in a grid-tied PV–battery charging station," *IEEE Trans. Ind. Inform.*, vol. 17, no. 10, pp. 6994–7004, Oct. 2021.

[24] E. Sortomme and M. A. El-Sharkawi, "Optimal scheduling of vehicle-to-grid energy and ancillary services," *IEEE Trans. Smart Grid*, vol. 3, no. 1, pp. 351–359, March 2012.

[25] X. Xie, Y. Zhang, K. Meng, Z. Y. Dong, and J. Liu, "Emergency control strategy for power systems with renewables considering a utility-scale energy storage transient," *CSEE J. Power Energy Syst.*, vol. 7, no. 5, pp. 986–995, Sep. 2021.

[26] J. P. F. Trovão, V. D. N. Santos, C. H. Antunes, P. G. Pereirinha and H. M. Jorge, "A real-time energy management architecture for

multisource electric vehicles," *IEEE Trans. Ind. Electron.*, vol. 62, no. 5, pp. 3223–3233, May 2015.
[27] J. Neubauer, and E. Wood, "The impact of range anxiety and home, workplace, and public charging infrastructure on simulated battery electric vehicle lifetime utility," *J. Power Sources*, vol. 257, no. 3, pp. 12–20, Jul. 2014.
[28] Z. Zhang, C. Dou, D. Yue, Y. Zhang, B. Zhang and B. Li, "Regional coordinated voltage regulation in active distribution networks with PV-BESS," *IEEE Trans. Circuits-II*, vol. 70, no. 2, pp. 596–600, Feb. 2023.
[29] M. Dehghani, E. Trojovska, P. Trojovsky, |and Z. Montazeri, "Coati optimization algorithm: a new bio-inspired metaheuristic algorithm for solving optimization problems," *Knowl-Based Syst.*, vol. 259, Art. no. 110011, Jan. 2023.

**Weixing Ma** received the B.S. degree in electrical engineering from Chongqing University of Posts and Telecommunications, Chongqing, China, in 2022. He is currently pursuing the M.S. degree in electrical engineering at Chongqing University of Posts and Telecommunications, Chongqing. His research interests include machine learning, pattern recognition, and economic dispatch involved in the fields of vehicle-grid integration, microgrid and new energy power system.

**Yiwei Ma** received the M.S. degree in control engineering (2007) and the Ph.D. degree in electrical engineering (2015) from South China University of Technology in China, and the B.Sc. degree (2003) from Yanshan University. In 2015, She joined Chongqing University of Posts and Telecommunications, where she is currently an Associate Professor of Electrical Engineering, and conduct more research on microgrid, smart grid, V2G and related technologies.

**Fuchun Deng** received the M.S. degree in control engineering (2021) from Chongqing University of Posts and Telecommunications in China. In 2021, He joined Chongqing College of Finance and Economics, where he is currently the professional leader of the Intelligent Product Development at Chongqing College of Finance and Economics, Chongqing, China. His main research fields are smart grid dispatching, intelligent control, and uncertainty research.